**Journal of the Earth and Space Physics, Vol. 47, No. 4, Winter 2022, P. 99-110 (Research)**

**DOI:** 10.22059/JESPHYS.2021.325291.1007330

# 3D Electromagnetic Low Induction Number Modeling using Integral Equations

Varfinezhad, R.[1*] and Parnow, S.[1]

1. *Ph.D. Graduated, Department of Earth Physics, Institute of Geophysics, University of Tehran, Tehran, Iran*

*(Received: 13 June 2021, Accepted: 20 Sep 2021)*

## Abstract

In this paper, a code for 3D forward modeling of electromagnetic low induction number (EM-LIN) data is developed based on the linear integral equations (IE). At first, the code is manipulated for a resistive block immersed in a homogenous background, and the obtained results have RMS errors of 2% comparing with the previously standard published results, which demonstrates the productivity of the 3D forward modeling code. Then, a model composed of two conductive anomalies with different depth ranges and conductivities in a resistive background is considered. IE Forward reposes shows that the shallower block produce larger values in spite of having less conductivity.

Since the forward modeling is linear, the productivity of the forward modeling code depends on the efficiency of the forward operator. Furthermore, linear forward operator plays the key role in the linear inversion procedure, therefore, a real data set of a thick dyke in Bloemfontein Nature Reserve region in South Africa is manipulated. Weighted damped minimum length solution is utilized for the inversion procedure and the inverted model is demonstrative of the forward operator efficiency in practical applications.

**Keywords:** Conductivities, EM-LIN, EM-34, 3D Forward modeling, IE, Inversion.

## 1. Introduction

Forward modeling has a vital role in geophysics because of I) its implementation in inversion procedure (Jahandari and Farquharson, 2013) and II) its application to investigate if recovered features in inversion model are constrained by the measured data or not (Simpson and Bahr, 2005). Furthermore, if one is dealing with field campaign, some important questions about choosing the best data sampling interval, distance between profiles and having insight into some characteristics of anomaly can be achieved by forward modeling (Varfinezhad et al., 2020). Electromagnetic methods include wide ranges of techniques like magnetotellurics (MT), ground-penetrating radar (GPR), control source electromagnetics (CSEM), and very low frequency (VLF) methods. They have been implemented for different practical applications such as oil and gas (Constable and Srnka, 2007; Yuan et al., 2017; Schaller et al., 2018), mining (Carlson and Zonge, 1997; Smith, 2014), groundwater (Olorunfem et al., 1995; Siemon et al., 2009), environmental and geotechnical (Pellerin, 2002; Fitterman and Labson, 2005) investigations. EM-LIN method is classified as a CSEM technique in frequency domain and is a common method to investigate the conductivity distribution of the near surface structures.

Since the subsurface is generally three-dimensional and due to the importance of forward modeling mentioned above, 3-D forward modeling of EM-LIN is of interest here, and the linear IE method proposed by Pérez-Flores et al. (2012) is utilized. The main advantage of the IE method in comparison with the FD and FE methods is the fast and accurate simulation of the response in models with compact 2D or 3D bodies in a layered background, while its main limitation is that the background conductivity model must have a simple structure to allow for an efficient Green's function calculation (Zhdanov, 2002). Fortunately, the most widely used background models in resistivity explorations are formed by horizontally homogeneous layers (Zhdanov, 2002).

At first, the 3D code is applied to two different models. Then its accuracy is investigated via comparing with the result obtained by Méndez-Delgado et al. (1999) for the model of a resistive body in the homogeneous conductive background. As a real test, the efficiency of the forward operator will be probed by inverting the

*Corresponding author: ramin.varfi@ut.ac.ir

collected data of a thick dyke in Bloemfontein using weighted damped minimum length solution method. Forward operator in linear inversion plays the role of Jacobian matrix in nonlinear inversion and its accuracy is decisive for the good performance of the inversion procedure.

## 2. Methodology

A typical LIN instrument consists of a transmitter coil and a receiver coil. In this method, an alternating current, flowing in the transmitter coil, generates primary magnetic field ($H_P$) into subsurface and surface. In the presence of conductivity variations in subsurface, eddy currents will be generated. Subsequently, these currents produce a secondary magnetic field (Hs). Both parts of fields are recorded by the receiving coil (Rx) (Figure 1) (Parnow et al., 2021).

Usually, the ratio of the secondary to primary magnetic fields (called 'coupling ratio') measured at the receiver coil is recorded as its in-phase (IP) and out-of-phase (or quadrature-phase, QP) parts (Beamish, 2011) or under LIN conditions assumption. Apparent conductivity estimated from QP part (McNeill, 1980) is obtained by Equation (1):

$$\sigma_{aPart} = \frac{4}{\omega\mu_0 s^2}\left(\frac{H_s}{H_p}\right)_{quadrature\ component} \quad (1)$$

The induction number is defined as the ratio of the inter-coil spacing (s) to the skin depth (δ) (McNeill 1980):

$$\beta = \frac{s}{\delta} = \frac{s}{\sqrt{\frac{2}{\sigma\omega\mu_0}}} \quad (2)$$

The skin depth is defined as the depth at which the transmitted magnetic field's amplitude has fallen to 1/*e* (about 0.37) of the initial magnitude at a reference point (Sheriff, 2002) and is given by:

$$\delta = \sqrt{\frac{2}{\omega\mu_0\sigma}} = \frac{\sqrt{2}\mathrm{i}}{\gamma} \quad (3)$$

where $\omega = 2\pi f$ is the angular frequency and $f$ is the frequency, $\mu_0 = 4\pi \times 10^{-7}$ H/m is the magnetic permeability of free space and $\sigma$ is the conductivity.

The IP and QP components are either directly mapped at the survey area to perform a qualitative interpretation of the conductivity distribution (Yoder et al., 2001; Doolittle and Brevik, 2014; Heil and Schmidhalter, 2017), or inversion procedures of multi-frequency data sets are implemented to compute a conductivity model of the subsurface (Song and Kim, 2008; Pérez-Flores et al., 2012; Kamm et al., 2013; Parnow et al., 2021). For more information about apparent conductivity under LIN assumption, see Parnow et al. (2021) paper.

Geonics instruments that are classified depending on the transmitter-receiver (T-R) distance, operate under LIN assumptions and the instruments show apparent conductivity as output. Any of these T-R distances are corresponding to a given frequency, which can be observed in Table 1. Furthermore, Table 1 contains the effective depth of explorations for these EM-LIN techniques indicating that the exploration depth of vertical magnetic dipoles (VMD) is two times of horizontal magnetic dipoles (HMD).

**Table 1.** Different EM-LIN techniques and their effective depth of exploration in 1-D environments (McNeill, 1980).

| Effective Depth of Exploration (m) | | | | |
|---|---|---|---|---|
| Instrument | T-R separation (m) | Frequency (kHz) | HMD | VMD |
| EM-38 | 1 | 14.6 | 0.75 | 1.5 |
| EM-31 | 3.66 | 9.8 | 2.75 | 5.50 |
| EM-34 | 10 | 6.4 | 7.5 | 15 |
| | 20 | 1.6 | 15 | 30 |
| | 40 | 0.4 | 30 | 60 |

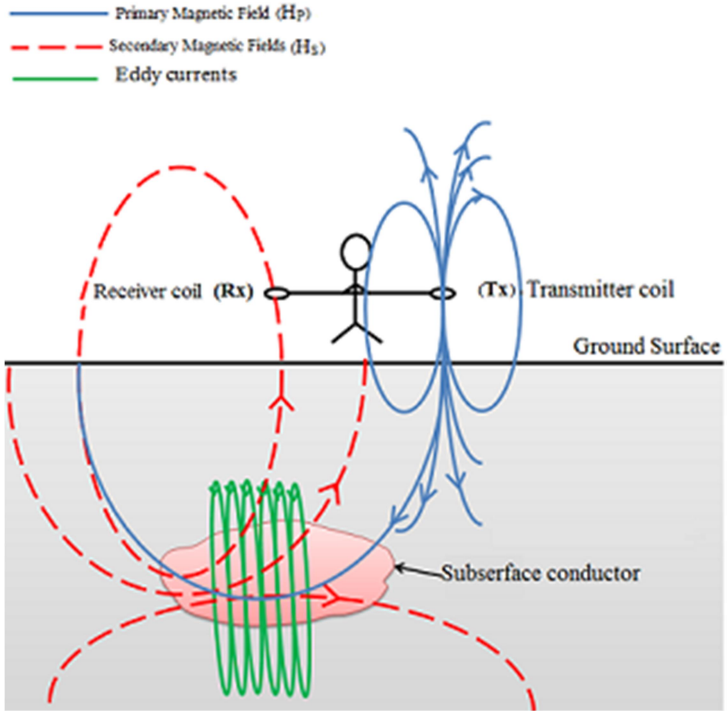


**Figure 1.** Sketch of LIN instrument in the presence of a heterogeneous earth. Time varying current in transmitter coil produced Hp (shown in blue color), Eddy currents are produced in the subsurface conductor (shown in green color), and finally Hs is produced by Eddy currents (shown in red color).

By exploiting Born approximation, Pérez-Flores et al. (2012) introduced the corresponding linear IEs for 3-D EM-LIN modeling of the horizontal and vertical magnetic dipoles. According to their method, observed apparent conductivity values are linearly related to the true conductivities as following equations for vertical magnetic dipoles (VMD):

$$\sigma_a(r_1,r_2) = -\frac{16\pi s}{\omega\mu_0 m_z}\iint_v G_{Hz}(r,r_2).E_{Hz}(r,r_1)\sigma(r)d^3r \quad (4)$$

and for horizontal magnetic dipoles (HMD)

$$\sigma_a(r_1,r_2) = -\frac{16\pi s}{\omega\mu_0 m_y}\iint_v G_{Hy}(r,r_2).E_{Hy}(r,r_1)\sigma(r)d^3r \quad (5)$$

where s is T-R separation, $\omega$ is angular frequency, $\mu_0$ is magnetic permeability, $m_z$ and $m_y$ are magnetic momentum around z and y direction, respectively. $\sigma_a$ and $\sigma(r)$ are in turn observed apparent conductivity and conductivity distribution of the subsurface. $r_1$, $r_2$ and $r$ are position vectors of transmitter, receiver and subsurface model, respectively (Figure 2-a). Relevant expressions for $G_{Hz}(r,r_2)$, $G_{Hy}(r,r_2)$, $E_{Hz}(r,r_1)$ and $E_{Hy}(r,r_1)$ are shown in Table 2.

For the numerical application, integral Equations (4) and (5) require to be discretized. For this reason, we discretize the subsurface into a lot of cells with the number of $n_x \times n_y \times n_z$ and side lengths of $lx$, $ly$ and $lz$ along x, y and z directions, respectively. It is assumed that the conductivity (resistivity) is constant inside each cell. By implementing this discretization on the integral Equations (4) and (5), both of them can be written as the following matrix formula:

$$d = Am \quad (6)$$

$d$, $A$ and $m$ are apparent conductivities (data vector), forward operator (kernel) and true conductivities (model vector), respectively. By applying the forward operator on a given model (known $m$), the forward modeling is made and apparent conductivities are obtained. In the next section, we are going to deal with this issue.

## 3. Numerical Results

In this section, the numerical results of applying 3-D forward modeling code on two different synthetic models are investigated: I) Resistive anomaly in a homogeneous

background, and II) multisource model including conductive anomalies.

### 3-1. Synthetic Case 1 (Resistive Anomaly)

The first synthetic case is a resistive anomaly placed at a depth range from 20 to 40 m and its horizontal extensions in x and y directions are 20 m (Figure 2-b). Conductivity values of the background and anomaly are 10 and 1 mS/m, respectively. The results of HMD derived by the 3-D code can be observed in Figure 3, while VMD responses are represented in Figure 4. In addition, forward response of both HMD and VMD with T-R=40 m and for all profiles are shown in Figure 5. Figure 3-a shows that with increasing the T-R separation, the apparent conductivity values obtained from manipulating the HMD array are decreased. Because of the depth range of the resistive block and the enhancement of depth of exploration by augmenting the T-R separation, this issue is expected and the observed data are more deviated from the background conductivity value toward lower conductivity. One important feature should be mentioned about the forward modeling results of the HMD array: for a resistive anomaly in the conductive background, the observed data values for all separations are equal to (in the leftmost and right most of the profiles) or less than (near to the position of the anomaly in the central part of the profile) the background conductivity value (10 mS/m). For the VMD array, increasing the T-R separation again results larger deviation from the background conductivity value, but for some separations (in this case s=1, 3.66 and 10 m) the observed conductivities are equal to (leftmost, rightmost and middle part of the profile) or less than (by approaching to the center of the profile) background conductivity, and for other separations (here s=20 and 40 m) less, equal and larger conductivity values relative to the background conductivity are observed. These numerical results are in a very good accuracy comparing with results derived by Méndez-Delgado et al. (1999) so that RMS errors of both are less than 2%. RMS error was computed according to the following formula:

$$RMS = \sqrt{\frac{\sum_{i=1}^{N}(d_i - d_{\ i}/d_i)^2}{N}} \times 100 \qquad (7)$$

where $d$ is data obtained by Méndez-Delgado et al. (1999) and $dc$ is computed data by 3D code, respectively, and $N$ is the number of data points.

**Table 2.** Magnetic dyadic Green's functions and electric field functions (Perez-Flores et al., 2012).

| |
|---|
| $$G_{H_z}(r,r_2) = \frac{1}{4\pi}\left[-\frac{(y-y_2)}{\lvert r-r_2\rvert^3}i + \frac{(x-x_2)}{\lvert r-r_2\rvert^3}j\right]$$ |
| $$E_{H_z}(r,r_1) = \frac{\omega\mu_0 m_z}{4\pi}\left[-\frac{(y-y_1)}{\lvert r-r_1\rvert^3}i + \frac{(x-x_1)}{\lvert r-r_1\rvert^3}j\right]$$ |
| $$G_{H_y}(r,r_2) = \frac{1}{4\pi}\left\{\left[\frac{1}{\rho_2^2} - \frac{z+h}{\rho_2^2\lvert r-r_2\rvert} - \frac{2(y-y_2)^2}{\rho_2^4} + \frac{2(z+h)(y-y_2)^2}{\rho_2^4\lvert r-r_2\rvert} + \frac{(z+h)(y-y_2)^2}{\rho_2^2\lvert r-r_2\rvert^3}\right]i + \left[\frac{(x-x_2)(y-y_2)}{\rho_2^2}\left(\frac{2}{\rho_2^2} - \frac{2(z+h)}{\rho_2^2\lvert r-r_2\rvert} - \frac{z+h}{\lvert r-r_2\rvert^3}\right)\right]j\right\}$$ |
| $$E_{H_y}(r,r_2) = \frac{\omega\mu_0 m_y}{4\pi}\left\{\left[\frac{1}{\rho_1^2} - \frac{z+h}{\rho_1^2\lvert r-r_1\rvert} - \frac{2(y-y_1)^2}{\rho_1^4} + \frac{2(z+h)(y-y_1)^2}{\rho_1^4\lvert r-r_1\rvert} + \frac{(z+h)(y-y_1)^2}{\rho_1^2\lvert r-r_1\rvert^3}\right]i + \left[\frac{(x-x_1)(y-y_1)}{\rho_1^2}\left(\frac{2}{\rho_1^2} - \frac{2(z+h)}{\rho_1^2\lvert r-r_1\rvert} - \frac{z+h}{\lvert r-r_1\rvert^3}\right)\right]j\right\}$$ |

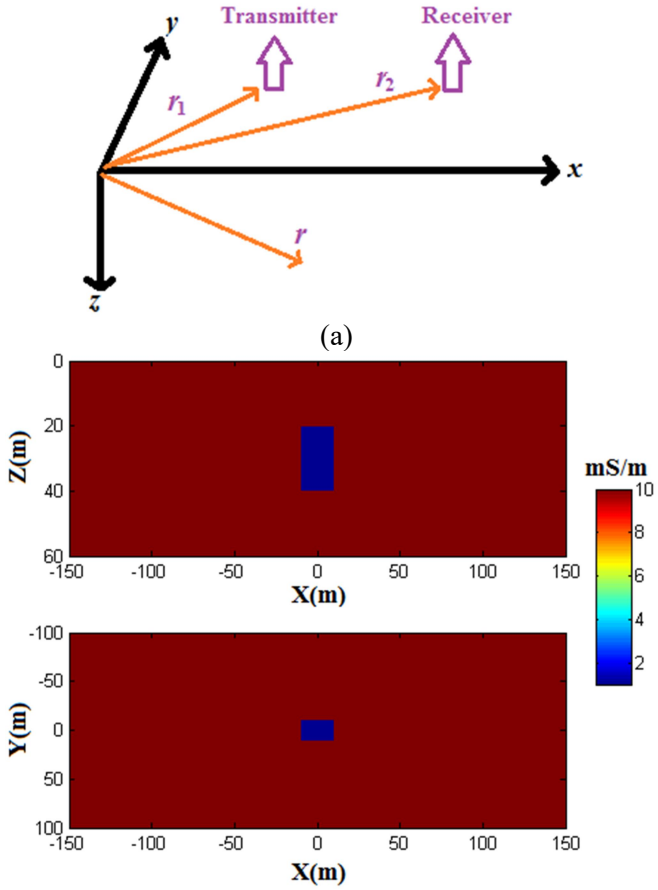


**Figure 2.** (a) Representation of transmitter, receiver and subsurface position vectors, and (b) model of the resistive block in a homogeneous background.

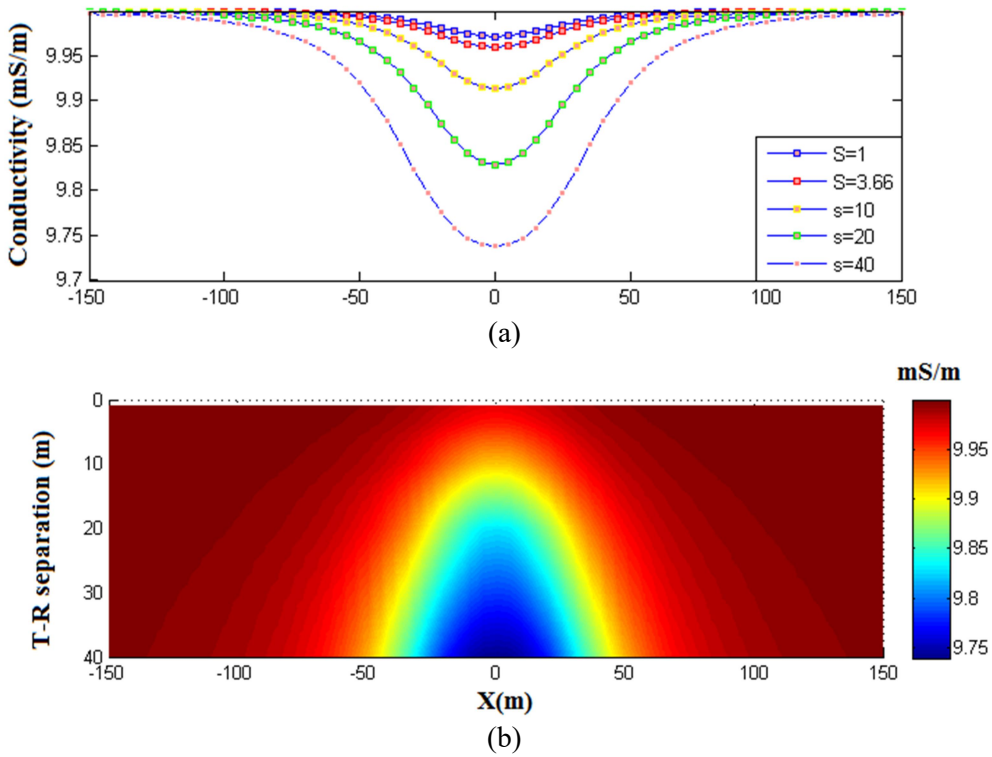


**Figure 3.** Computed forward response of HMD using the 3-D IE code for the central profile (y=0). (a) Plot of the computed data for each T-R separation, and (b) data pseudo-section derived from all T-R separations.

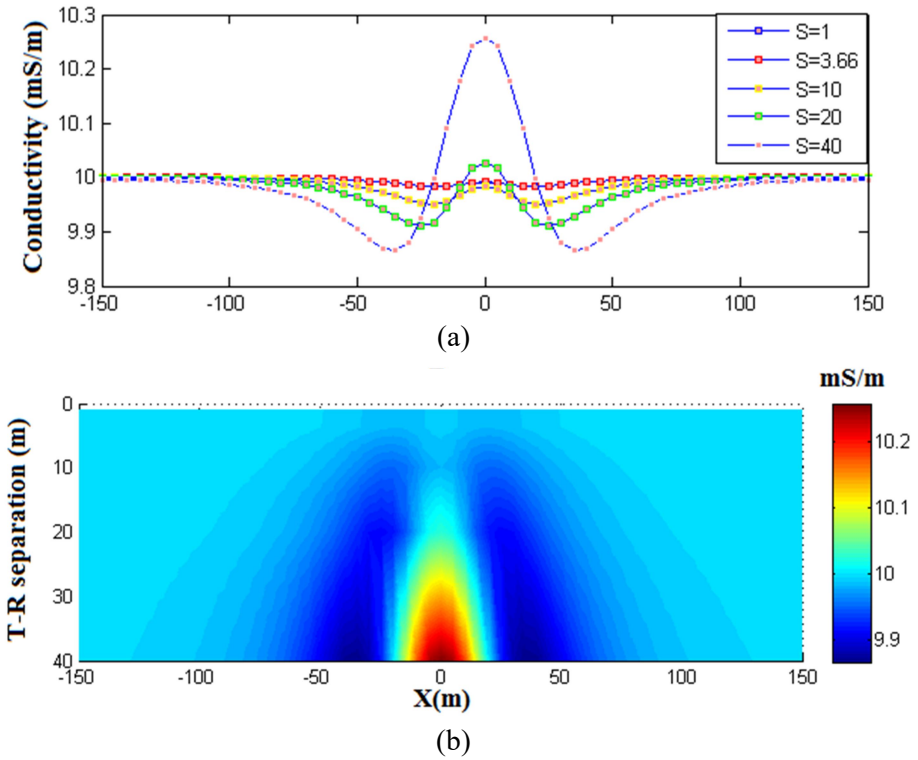


**Figure 4.** Computed forward response of VMD using the 3-D IE code for the central profile (y=0). (a) Plot of the computed data for each T-R separation, and (b) data pseudo-section derived from all T-R separations.

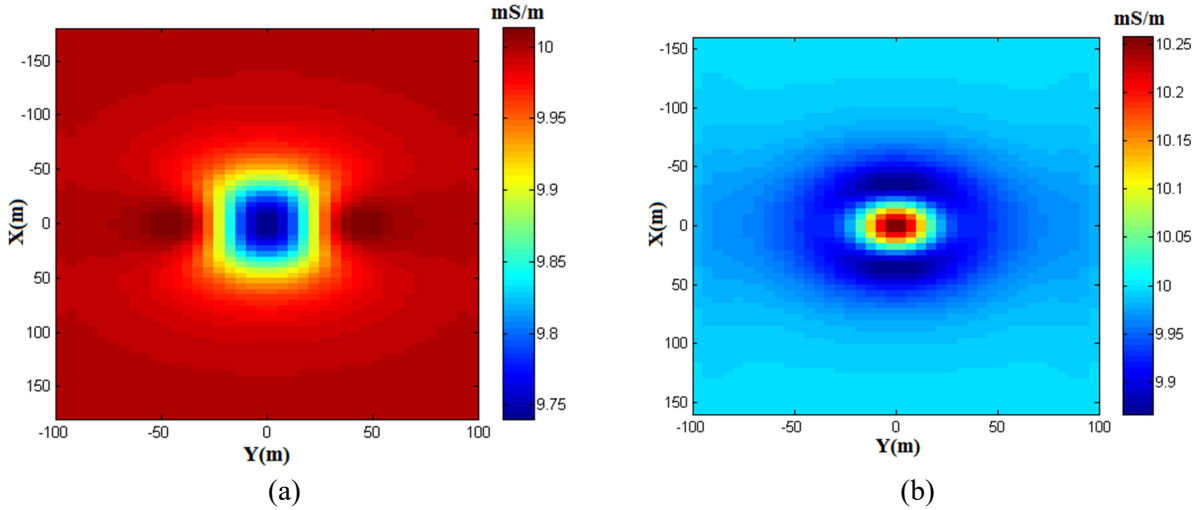


**Figure 5.** Representation of the forward responses of a) HMD and b) VMD techniques with T-R=40 m for all of the profiles.

### 3-2. Synthetic Case 2 (Conductive Anomalies)

For the second numerical example, a model composed of two conductive bodies immersed in a homogenous resistive background of 10 mS/m is considered (Figure 6). The characteristics of these two conductive bodies are specified in Table 3. Like the previous synthetic case, IE forward modeling code responses for the central profile (y=0) are shown for both HMD and VMD arrays (Figure 7 and Figure 8). For both arrays, it can be observed that the obtained apparent conductivities are not significantly different with background value (10 mS/m) for T-R separation of 1 and 3.66 m that is expected due to the block depth ranges. Increasing the T-R separation leads to significant anomalies for both arrays but with two

differences: I) obtained values from VMD array are larger than HMD array, which is consistent with the more effective depth of exploration of the VMD array, II) HMD are always larger than the background value of conductivity, but VMD array can produce values significantly smaller than the background conductivity.

**Table 3.** Characteristics of the two conductive anomalies surrounded by the resistive background of 10 mS/m.

| anomaly | X (m) | Y(m) | Z(m) | Conductivity (mS/m) |
|---|---|---|---|---|
| Shallower | From -35 to -15 | From -20 to 20 | 10-30 | 30 |
| Deeper | From 15 to 35 | From -20 to 20 | 20-40 | 50 |

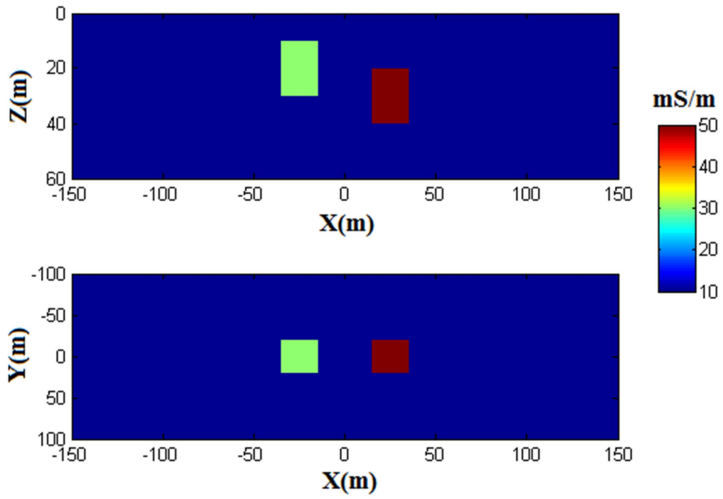


**Figure 6.** Model of the two conductive blocks with different conductivities surrounded by homogeneous medium.

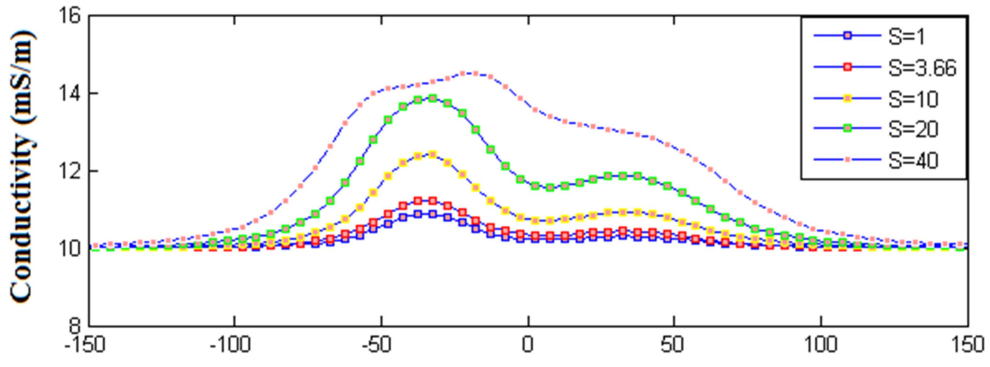


(a)

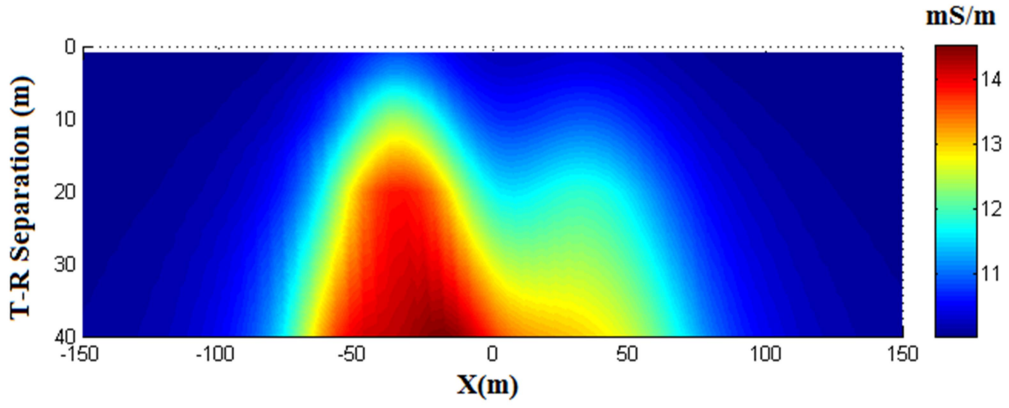


(b)

**Figure 7.** Computed forward response of HMD using the 3-D IE code for the central profile (y=0). (a) Plot of the computed data for each T-R separation and (b) data pseudo-section derived from all T-R separations.

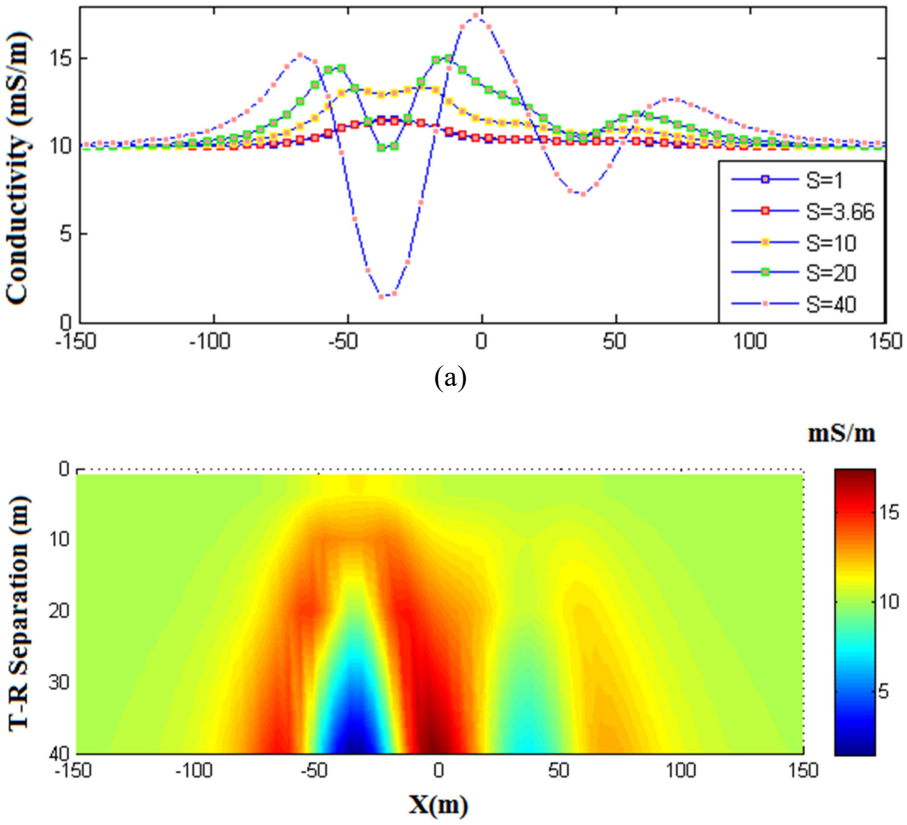


**Figure 8.** Computed forward response of VMD using the 3-D IE code for the central profile (y=0). (a) Plot of the computed data for each T-R separation and (b) data pseudo-section derived from all T-R separations.

## 4. Real Data

In the previous section, two synthetic examples of forward modeling were presented. The efficiency of the forward modeling depends on the forward operator **A** accuracy. This forward operator plays the role of jacobian matrix in linear inversion. Therefore, a real test may be made through inverting a real data set utilizing this forward operator. Since the available data set is only one profile, it is appropriate for 2-D inverse modeling. In order to prepare the forward operator for the 2-D inversion, it is required to integrate the Equations (4) and (5) from minus infinity to infinity. By doing this process, the problem is 2-D modeling and we have the corresponding 2-D forward operator.

Inversion procedure is made using the weighted damped minimum length solution with respect to an initial homogenous model assuming to be equal to the mean value of the measured apparent conductivities. Like other geophysical methods, EM-LIN data inversion suffers from non-uniqueness and instability, so introducing constraints is necessary to obviate these problems. Minimizing the following objective function (Tikhonov and Arsenin, 1977) leads to the inversion solution of the linear system of Equation (6):

$$\min \rightarrow \|\boldsymbol{W}_d(\boldsymbol{Am}-\boldsymbol{d})\|_2^2+\alpha\|\boldsymbol{W}_m(\boldsymbol{m}-\boldsymbol{m}_a)\|_2^2 \quad (8)$$

where $\boldsymbol{m}_a$ is the initial model, $\alpha$ is regularization parameter and $\boldsymbol{W}_d$ and $\boldsymbol{W}_m$ are data and model weighting matrices, respectively. We assume that $\boldsymbol{W}_d$ to be the identity matrix. Solving Equation (8) can lead to the following weighted damped minimum length solution (Menke, 2012):

$$\boldsymbol{m}=\boldsymbol{m}_r+(\boldsymbol{W}_m^{-1}\boldsymbol{A}^T)(\boldsymbol{A}\boldsymbol{W}_m^{-1}\boldsymbol{A}^T+\alpha I)^{-1}(\boldsymbol{d}-\boldsymbol{A}\boldsymbol{m}_r) \quad (9)$$

$\boldsymbol{W}_m$ is depth weighting matrix introduced by Li and Oldenburg (1996) for the 3-D inversion of the magnetic data as the following formula:

$$\boldsymbol{W}_z=\frac{1}{(\boldsymbol{Z})^{(\beta/2)}} \quad (10)$$

$\boldsymbol{Z}$ is the vector of cell center coordinates and $\beta$ is the depth weighting exponent.

EM 34 data was collected on a thick conductive dyke in Bloemfontein Nature Reserve region in South Africa. The area is dominated by fine sandstone and siltstone (Makhokha and Fourie, 2016). Data of both HMD and VMD arrays may be observed in Figure 9, while the inversion model obtained from this data set is represented in Figure 10-a. The inversion model is suggestive of a thick conductive dyke, the horizontal extension of which is from 120 m to 180 m, and its depth extension is from near surface (about 4 m) to 20 m. Furthermore, the left side of the subsurface is more resistive than the right side, and this can be interpreted qualitatively from the measure data. For the iterative inversion process, the depth weighting exponent, the regularization parameter and the number of iterations are, in turn, 2, 1 and 6. Lower bound and upper bounds applied on the model conductivity values were 3 and 100, respectively. In conclusion, this real test is indicative of satisfactory performance of the forward operator.

Figure 10-b shows the trend of misfit RMS error with iteration number indicating that misfit RMS error decreases insignificantly from iteration number 5 to 6 (about 0.2%); therefore, the iterative inversion procedure was stopped and the inversion model derived from iteration number 6 was adopted as the final model. Initial estimation of regularization parameter was made according to one tenth of the maximum value of the kernel matrix (0.1×Max(A)=0.1×27=2.7), then we changed it slightly during four trial and errors, and finally it was fixed to be 1. In the following investigation that is dealing about the inversion of EM-LIN data, the estimation of regularization parameter using this technique is one of the main issues that will be discussed. Another critical issue about the suggested inversion algorithm (Equation (9)) is determination of the depth weighting exponent, which should be investigated comprehensively; therefore, the inversion modeling of EM-LIN data and adoption inverse parameters requires an exhaustive examination using both synthetic and other real data sets, which is beyond the scope of this paper.

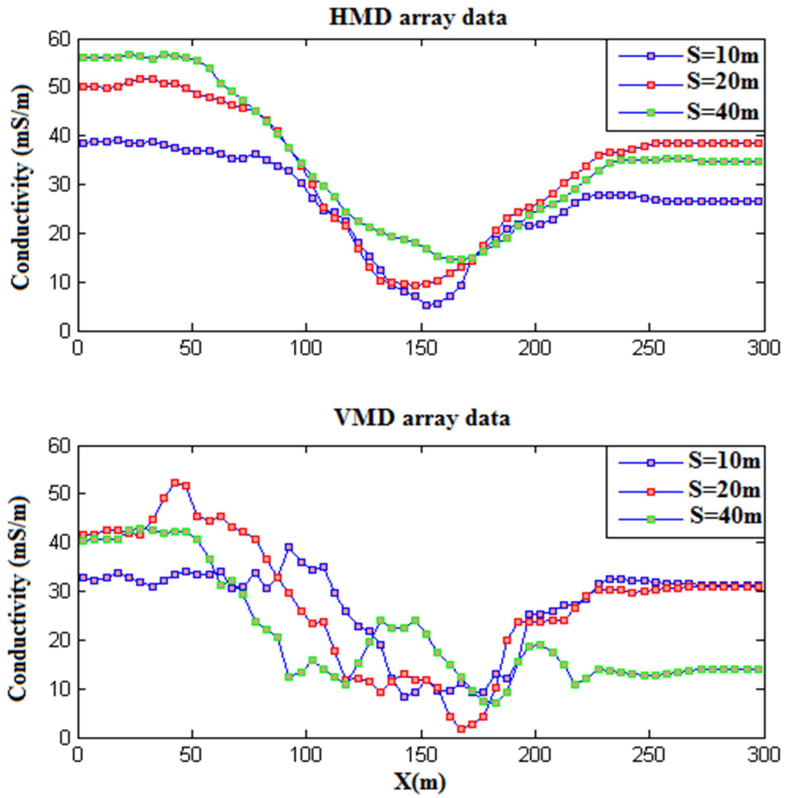


**Figure 9.** Data collected in Bloemfontein.

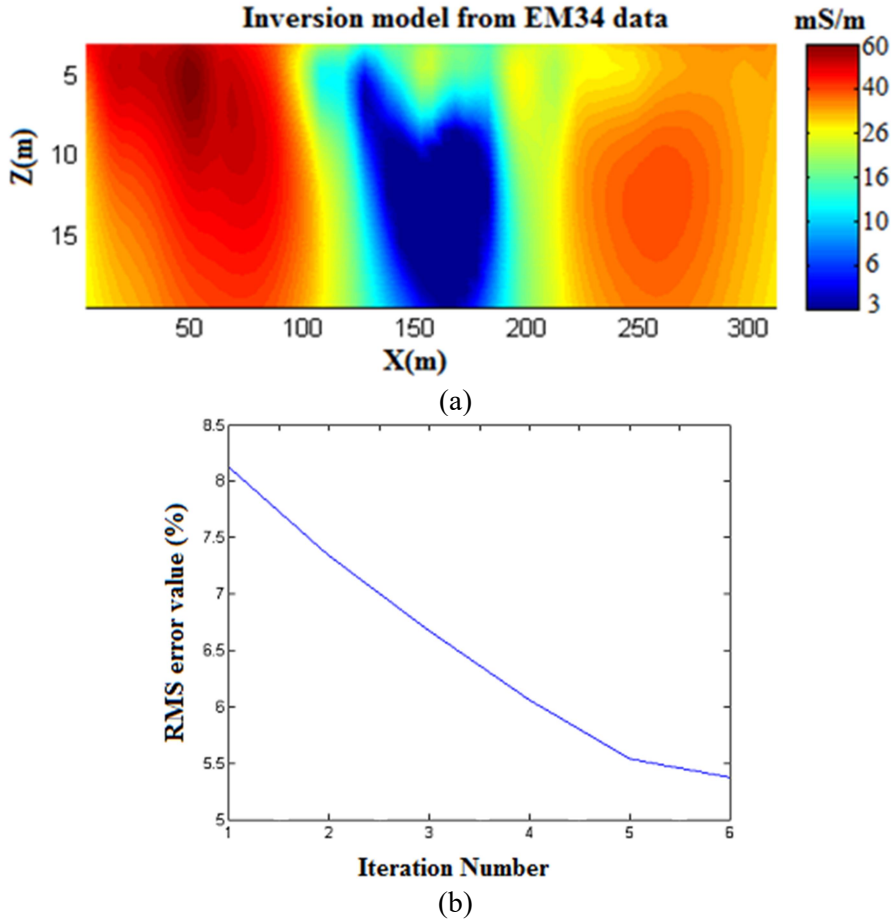


**Figure 10.** (a) Inversion model derived from the measured data shown in the previous figure. (b) trend of misfit RMS error with iteration number.

## 5. Conclusions

3D modeling of EM-LIN method using linear integral Equation was dealt with in this paper. Two synthetic cases were considered: I) a resistive block in a homogenous medium for which the result derived from our code has an RMS error of less than 2% comparing with previously published results indicating the productivity of our code, II) two conductive anomalies with different depth ranges and conductivities immersed in a homogenous background. According to the obtained results, for HMD array, the deviation of the forward response from background value is less (for resistive anomaly) and larger (for conductive anomaly) than this background value for all T-R separations. For VMD, the deviation can be less and larger for resistive or conductive anomaly. In order to show the efficacy of the forward operator practically, a profile of a real data set was manipulated to be inverted by the corresponding 2-D forward operator, which was computed using integration of the 3-D formula along y axis from minus infinity to infinity, and the retrieved model from the inversion procedure demonstrated the reliability of the forward operator for practical application.

## Acknowledgements

We would like to thank Dr. Dakalo Makhokha for providing the LIN EM34 data.

## References

Beamish, D., 2011, Low induction number, ground conductivity meters: A correction procedure in the absence of magnetic effects, Journal of Applied Geophysics 75(2), 244-253.

Carlson, N. R. and Zonge, K. L., 1997, Case histories of electrical and electromagnetic geophysics for environmental applications at active mines. 10th EEGS Symposium on the Application of Geophysics to Engineering and Environmental Problems, European Association of Geoscientists & Engineers.

Constable, S. and Srnka, L. J., 2007, An introduction to marine controlled-source electromagnetic methods for hydrocarbon exploration, Geophysics 72(2), WA3-WA12.

Doolittle, J. A. and Brevik, E. C., 2014, The use of electromagnetic induction techniques in soils studies, Geoderma 223, 33-45.

Fitterman, D. V. and Labson, V. F., 2005, Electromagnetic induction methods for environmental problems. Near-surface geophysics, Society of Exploration Geophysicists, 301-356.

Heil, K. and Schmidhalter, U., 2017, The application of EM38: Determination of soil parameters, selection of soil sampling points and use in agriculture and archaeology, Sensors 17(11), 2540.

Jahandari, H. and Farquharson, C. G., 2013, Forward modeling of gravity data using finite-volume and finite-element methods on unstructured grids, Geophysics 78(3), G69-G80.

Kamm, J., Becken, M. and Pedersen, L. B., 2013, Inversion of slingram electromagnetic induction data using a Born approximation, Geophysics 78(4), E201-E212.

Li, Y. and Oldenburg, D. W., 1996, 3-D inversion of magnetic data, Geophysics 61(2), 394-408.

Makhokha, D. and Fourie, F., 2016, A systematic approach to the interpretation of conductivity anomalies across intrusive dolerite dykes and sills in the Karoo Supergroup, MSc thesis. University of the Free State, Bloemfontein.

McNeill, J. D., 1980, Electromagnetic terrain conductivity measurement at low induction numbers.

Méndez-Delgado, S., Gómez-Treviño, E. and Pérez-Flores, M. A., 1999, Forward modelling of direct current and low-frequency electromagnetic fields using integral equations, Geophysical Journal International 137(2), 336-352.

Menke, W., 2012, Geophysical data analysis: discrete inverse theory: MATLAB edition, Academic press.

Olorunfem, M. O., Dan-Hassan, M. A. and Ojo, J. S., 1995, On the scope and limitations of the electromagnetic method in groundwater prospecting in a Precambrian basement terrain-a Nigerian case study, Journal of African Earth Sciences 20(2), 151-160.

Parnow, S., Oskooi, B. and Florio, G., 2021, Improved linear inversion of low induction number electromagnetic data, Geophysical Journal International 224(3), 1505-1522.

Pellerin, L., 2002), Applications of electrical and electromagnetic methods for environmental and geotechnical investigations, Surveys in Geophysics 23(2), 101-132.

Pérez-Flores, M. A., Antonio-Carpio, R. G., Gómez-Treviño, E., Ferguson, I. and Méndez-Delgado, S., 2012, Imaging of 3D electromagnetic data at low-induction numbers, Geophysics 77(4), WB47-WB57.

Schaller, A., Streich, R., Drijkoningen, G., Ritter, O. and Slob, E., 2018, A land-based controlled-source electromagnetic method for oil field exploration: An example from the Schoonebeek oil field, Geophysics 83(2), WB1-WB17.

Sheriff, R. E., 2002, Encyclopedic dictionary of applied geophysics, Society of exploration geophysicists.

Siemon, B., Christiansen, A. V. and Auken, E., 2009, A review of helicopter-borne electromagnetic methods for groundwater exploration, Near Surface Geophysics 7(5-6), 629-646.

Simpson, F. and Bahr, K., 2005, Practical magnetotellurics, Cambridge University Press.

Smith, R., 2014, Electromagnetic induction methods in mining geophysics from 2008 to 2012, Surveys in Geophysics 35(1), 123-156.

Song, Y. and Kim, J.-H., 2008, An efficient 2.5 D inversion of loop-loop electromagnetic data, Exploration Geophysics 39(1), 68-77.

Tikhonov, A. N. and Arsenin, V. Y., 1977, Solutions of ill-posed problems, New York 1(30), 487.

Varfinezhad, R., Oskooi, B. and Fedi, M., 2020, Joint Inversion of DC Resistivity and Magnetic Data, Constrained by Cross Gradients, Compactness and Depth Weighting, Pure & Applied Geophysics 177(9).

Yoder, R. E., Freeland, R. S., Ammons, J. T.

and Leonard, L. L., 2001, Mapping agricultural fields with GPR and EMI to identify offsite movement of agrochemicals, Journal of Applied Geophysics 47(3-4), 251-259.

Yuan, B., Li, D. and Bayless, R. C., 2017, Wide field electromagnetic method for shale gas exploration in southern China: A case study, Journal of Environmental and Engineering Geophysics 22(3), 279-289.

Zhdanov, M. S., 2002, Geophysical inverse theory and regularization problems, Elsevier.